






Compact Triangular-Cavity Singlet-Based Filters in Stackable Multilayer Technologies

Chad Bartlett , *Graduate Student Member, IEEE*, Mohammad Mehrabi Gohari ,
Oleksandr Glubokov , *Member, IEEE*, Joachim Oberhammer , and Michael Höft , *Senior Member, IEEE*

Abstract—In this letter, triangular-cavity bandpass filters are investigated in stackable multilayer technologies in order to achieve highly compact designs with reduced fabrication complexity. The triangular-shaped cavities are first introduced in the form of singlets and then expanded on as a novel method for achieving a quasi-triplet filter response, where the filter’s input and output irises are utilized as resonating means for two additional passband poles. Exploitation of this advanced singlet scheme exemplifies innovative use of resonant irises for achieving highly compact filters that can be manufactured with simple multilayer fabrication steps for use in future terahertz applications.

Index Terms—Deep reactive ion etching (DRIE), electrical-discharge machining (EDM), resonant iris, singlet, triangular cavity, wire erosion.

I. INTRODUCTION

AS TRENDS for high-frequency applications rise, technologies must evolve to sustain current demands as well as prepare for future ones. For the next generation of satellite communications, radar, and deep-space exploration, filter designs must be continuously adapted to optimize performance while the allocation of frequency bands reaches beyond the radio-frequency spectrum. Although, different technologies, such as high-precision milling [1], SU-8 [2], silicon micromachining [3], and structured glass [4], have been able to demonstrate the ability to reach well into the terahertz and subterahertz regions, progressive design solutions must be continuously explored to coincide with technological advancements.

In order to facilitate future demands for the aforementioned applications, novel designs must be considered for very high-frequency regions where the effect of dimensional tolerances becomes critical, the ability to tune circuits diminishes, and the constraints imposed on size and weight become highly

Manuscript received 20 May 2022; revised 4 July 2022; accepted 12 July 2022. Date of publication 15 July 2022; date of current version 3 September 2022. This work was supported in part by the European Union’s Horizon 2020 Research and Innovation Programme under the Marie Skłodowska-Curie under Grant 811232-H2020-MSCA-ITN-2018. (Corresponding author: Chad Bartlett.)

Chad Bartlett and Michael Höft are with the Department of Electrical and Information Engineering, University of Kiel, 24118 Kiel, Germany (e-mail: chb@tf.uni-kiel.de; mh@tf.uni-kiel.de).

Mohammad Mehrabi Gohari, Oleksandr Glubokov, and Joachim Oberhammer are with the Department of Micro and Nanosystems, KTH Royal Institute of Technology, SE 100 44 Stockholm, Sweden (e-mail: mohmg@kth.se; glubokov@kth.se; joachimo@kth.se).

Color versions of one or more figures in this article are available at <https://doi.org/10.1109/TTHZ.2022.3191237>.

Digital Object Identifier 10.1109/TTHZ.2022.3191237

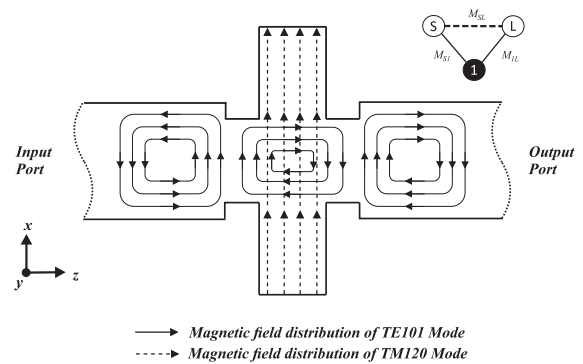


Fig. 1. Magnetic field distribution of Singlet 1 with depiction of the bypass coupling through the triangular cavity. Filter topology: source/load nodes are white and the resonating node is black. Solid lines are the main path while the dashed line is the bypass path.

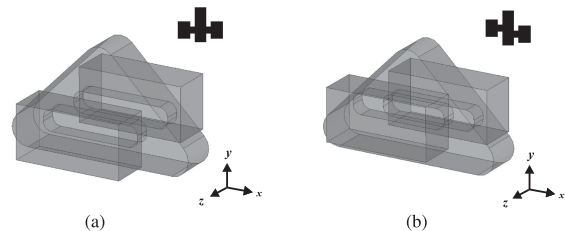


Fig. 2. Vacuum shell of (a) Singlet 1 and (b) Singlet 2. The inset images depict the side views of each singlet’s input positions, either inline or offset.

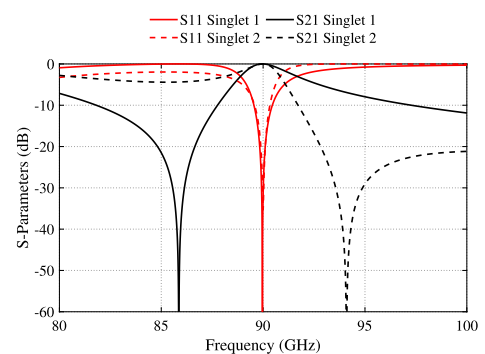


Fig. 3. Simulated results of Singlet 1 and Singlet 2 from Fig. 2.

consequential. In the case of compact high-frequency designs, research works conducted, such as [3], [5], and [6], have been able to demonstrate the ability to minimize the overall footprint of structures, remove the need for lengthy input/output feeding

transitions, and in some cases, employ resonant irises to enhance the filter response. Moreover, the introduction of filters with singlets have gained much attention in the literature due to their relatively small size, simple design, and their ability to easily control transmission zero locations [7]–[9]. Extension of this concept to a variety of different resonator types and filtering operations are exemplified in papers, such as [10]–[16].

In regards to simple manufacturing procedures for millimeter and submillimeter wave filter components, stackable technologies and multilayer designs have been demonstrated using methods, such as electronic-band-gap [17], diffusion bonding of laminated metal plates [18], deep reactive ion etching (DRIE) [3], [5], and structured-glass waveguide components [4]. However, miniaturization methods at the millimeter and submillimeter wave bands becomes increasingly difficult due to highly stringent dimensions combined with the need for precise alignment of multiple structural layers. In this letter, we propose a simple and elegant design scheme for compact bandpass filters with three stackable layers using an advanced singlet topology. The formulation utilizes a triangular cavity singlet that is combined with two resonant slot-type irises in order to create a third-order bandpass response with one transmission zero, resulting in a quasi-triplet filter topology. In order to verify the proposed filter scheme, a prototype is demonstrated using electrical-discharge machining (EDM) for W-band (75–110 GHz) operation, while a second prototype is demonstrated in DRIE for J-band (220–330 GHz) operation. Each of the bandpass filter iterations demonstrates a highly compact and simple fabrication scheme that is suitable for future terahertz applications.

II. FILTER DESIGN

The singlet is a first-order topology that is capable of generating a transmission zero either above or below the frequency location of the pole, where the position of the transmission zero depends on the sign of the bypass coupling. In this regard, the transmission zero can be modeled on the lower side of the stopband when $M_{sl} < 0$, and on the upper side of the stopband when $M_{sl} > 0$, [16].

Advancements in triangular waveguide structures, such as the analysis provided in [19]–[21], allow for the application of singlet theory to be extended to shapes beyond typical rectangular or circular cavities and formulated for the evolution of triangular-shaped filter structures. As outlined in [19], the resonant frequency of an isosceles triangular cavity can be found from

$$f_{mn} = \frac{1}{2a\sqrt{\mu\epsilon}} \sqrt{m^2 + n^2} \quad (1)$$

where $m = 0, 1, 2, \dots$, $n = 0, 1, 2, \dots$, and $m + n \neq 0$. Using (1), we can characterize triangular-waveguide singlets and quasi-triplets operating with the TM120 mode for the first time in the literature as an alternative geometry—which is also convenient for optimizing on-chip layout—and is capable of achieving an equivalent Q-factor via (1) when compared with rectangular or cylindrical cavities that have similar thicknesses and center frequencies, and operate with analogous electromagnetic field distributions (i.e., the TM110 and TM010 modes, respectively).

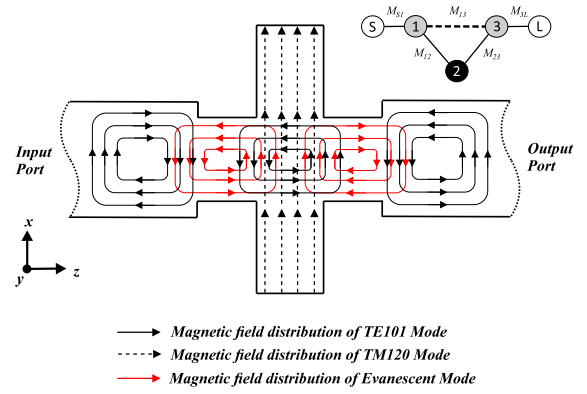


Fig. 4. Magnetic field distribution of the triangular-cavity filter with depiction of the bypass coupling and resonant slot irises. Filter topology: source/load nodes are white, resonating irises are gray, and the resonating node is black. Solid lines are the main path while the dashed line is the bypass path.

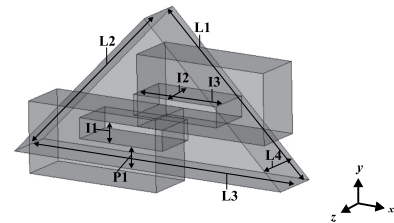


Fig. 5. Vacuum shell of the proposed filter. The corresponding dimensions (in mm) for WR-10— $L1=3.800$, $L2=3.800$, $L3=5.374$, $L4=0.900$, $I1=0.400$, $I2=0.800$, $I3=1.660$, and $P1=0.645$ —and WR-3— $L1=1.287$, $L2=1.287$, $L3=1.821$, $L4=0.308$, $I1=0.117$, $I2=0.278$, $I3=0.564$, and $P1=0.234$. Values are rounded to three decimal places. An estimated underetching between 4.25 and 6.10 μm should be applied to the WR-3 version.

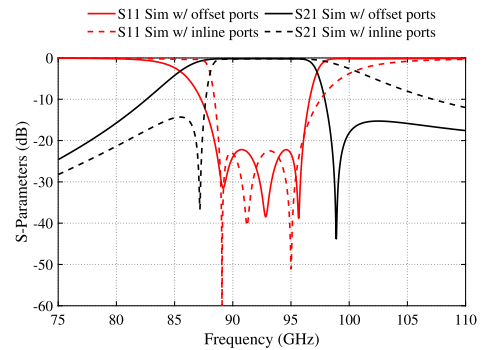


Fig. 6. Simulated demonstration of the transmission zero control when varying the positions of the triangular-cavity filter ports to be inline or offset. The cavity dimensions and resonant slot irises are optimized for a comparable passband response.

For the design at hand, we select the TM120 mode and formulate the singlet to be fed with slot-type irises in a position that can simultaneously allow for a bypass coupling to pass from the source to load; Fig. 1 depicts the magnetic field distribution for the 90 GHz triangular singlet example that follows in Fig. 2(a). In addition, the singlet topology is indicated in the image for reference. Fig. 2(a) and (b) shows two cases of a singlet, which is designed for operation at 90 GHz where the transmission zero position is selected relative to the positions of the source/load coupling; inline or offset. The structure proposed

in Fig. 2(a) results in the transmission zero on the lower side ($M_{sl} < 0$), while the structure proposed in Fig. 2(b) results in the transmission zero on the upper side ($M_{sl} > 0$). This effect is demonstrated in Fig. 3 for the simulation of each structure over 80–100 GHz.

In order to extend this concept to bandpass filter design, the triangular singlet can be modified to include resonant irises similar to the formulations outlined in [22] and [23]. Fig. 4 shows the magnetic field distribution of a singlet with the two resonant irises and describes the basic interaction throughout the filter. The modified topology now includes the resonant irises and is indicated in the image for reference; it can be noted that the bypass coupling is now formed between the resonant slot irises (nodes 1 and 3) in a quasi-triplet fashion. The evanescent modes of the resonant slot irises can be treated as TE₁₀₁ modes while the triangular cavity (node 2) utilizes the TM₁₂₀ mode. Fig. 5 shows the vacuum shell of an inline quasi-triplet structure and outlines the dimensions for each of the upcoming prototypes when fed with their respective waveguide ports. Fig. 6 is provided as a demonstration of the transmission zero control when varying the port positions to be inline or offset while the triangular cavity and the resonant irises are optimized for an equivalent passband response.

After the initial design of the cavity from equation (1) for an isosceles cavity, the synthesis of the passband filter can be suitably approximated from the general equations outlined in [24] for external quality factors and synchronous coupling despite the resonant irises and cavity being asynchronous. This method is used as a good approximation; however, the structure can also be viewed in a transverse coupling matrix form for simple parameter extraction. In order to verify this concept, a third-order filter with a fractional bandwidth (FBW) and center frequency of approximately 7.2% and 91.7 GHz is specified for EDM wire erosion for WR-10 band operation, while another with a FBW and center frequency of approximately 5.4% and 268.9 GHz is specified for DRIE on silicon wafers for WR-3 band operation.

III. FABRICATION AND MEASUREMENTS

For the WR-10 version of the filter, wire erosion was selected for its ability to reduce the necessary corner radii within the structures. Brass was selected as the cutting material with an erosion wire of 60 μm radius. The filter is fabricated as three individual pieces, namely, brass plates that house the irises and the triangular cavity. For the WR-3 version of the filter, a standard silicon micromachining process based on DRIE has been employed for its ability to obtain micron-level detail and high repeatability. The fabrication has been performed on a silicon-on-insulator (SOI) wafer that consists of a 30 μm device layer, a 275 μm handle layer, and a 3 μm buried oxide layer. The proposed filter was built using three stacked layers while gold (Au) sputtering was used to metallize the chips. Each of the layers is aligned on top of one another using Vernier scale alignment marks before thermocompression bonding. To minimize the effect of underetching and promote a high accuracy between the simulated and measured results, the middle layer

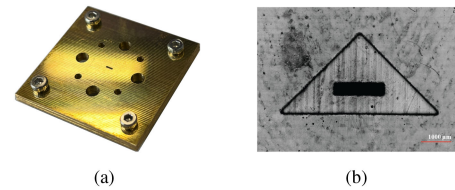


Fig. 7. Fabricated W-band prototype. (a) Assembled filter unit. (b) Close-up view of the internal cavity and one of the resonating iris slots.

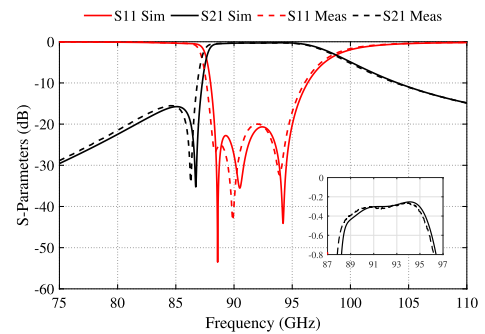


Fig. 8. Simulated versus measured S-parameter results of the stacked EDM filter for W-band operation. Effective conductivity is taken as 7.50 MS/m.

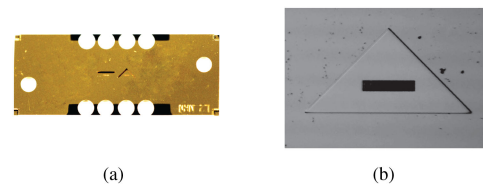


Fig. 9. Fabricated J-band prototype. (a) Chip layers one and two stacked on top of one another with two internal cavities shown. (b) Close-up view of an internal cavity and one of the resonating iris slots throughout the chip.

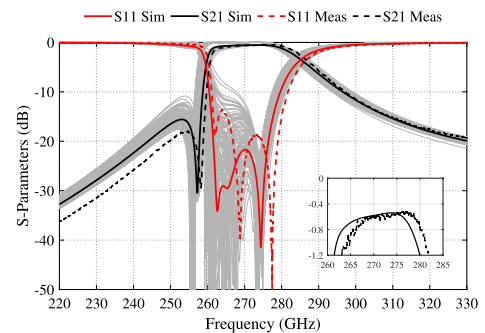


Fig. 10. Simulated versus measured S-parameter results of the stacked silicon wafer filter for J-band operation. Effective conductivity is taken as 10.8 MS/m. Gray lines indicate the tolerance analysis of 100 runs.

is fabricated using a fallout technique [25], and a compensative side wall underetching effect has been applied to the design.

Once fabricated and assembled, both versions of the filters were tested using a Rohde & Schwarz ZVA67 with their respective up-converters. Fig. 7 shows the fabricated structure from EDM wire erosion, while Fig. 8 shows a comparison of the simulated and measured results over 75–110 GHz. The measured return loss is better than 20 dB in the measured passband while

the measured insertion loss at the measured center frequency is approximately 0.31 dB with an estimated Q_u of ≈ 500 . Fig. 9 presents the fabricated structure from DRIE micromachining, while Fig. 10 presents a comparison of the simulated and measured results over 220–330 GHz. The measured return loss is better than 13.5 dB in the measured passband and the measured insertion loss at the measured center frequency is approximately 0.61 dB with an estimated Q_u of ≈ 300 . A tolerance analysis comparing 100 runs with Gaussian randomized points within $\pm 2 \mu\text{m}$ is added to the figure. However, some mismatch may be attributed to the underetching effect caused by DRIE and may be compensated in further iterations. The WR-10 and WR-3 L·W·H internal dimensions are approximately $0.764 \cdot 1.588 \cdot 0.814 \lambda^3$ and $0.864 \cdot 1.821 \cdot 0.815 \lambda^3$, respectively.

IV. CONCLUSION

In this work, the concept of triangular-cavity singlets combined with resonant irises is explored in order to achieve novel bandpass filters in stackable multilayer technologies. Prototypes of the filter concept are designed and measured for high-frequency applications in the WR-10 and WR-3 bands with wire erosion and silicon wafer technology, respectively. The introduction of singlets with slot-type resonant irises demonstrates a versatile approach for compact filter design suitable for future terahertz applications.

REFERENCES

- [1] J.-Q. Ding et al., “WR-3 band quasi-elliptical waveguide filters using higher order mode resonances,” *IEEE Trans. THz Sci. Technol.*, vol. 7, no. 3, pp. 302–309, May 2017.
- [2] X. Shang et al., “SU-8 micromachined cross-coupled waveguide cavity filter for sideband rejection above 300 GHz,” in *Proc. 10th U.K.-Eur.-China Workshop Millimetre Waves THz Technol.*, 2017, pp. 1–2.
- [3] O. Glubokov et al., “Micromachined multilayer bandpass filter at 270 GHz using dual-mode circular cavities,” *Proc. IEEE MTT-S Int. Microw. Symp.*, Honolulu, USA, 2017, pp. 1449–1452.
- [4] C. Bartlett, A. Malavé, M. Letz, and M. Höft, “Structured-glass waveguide technology for high-performance millimetre wave components and subsystems,” *IEEE J. Microw.*, vol. 2, no. 2, pp. 307–315, Apr. 2022.
- [5] X. Zhao, O. Glubokov, U. Shah, and J. Oberhammer, “Highly compact silicon micromachined filter with axial ports at sub-terahertz band,” in *Proc. Asia-Pacific Microw. Conf.*, 2019, pp. 768–770.
- [6] X. Shang et al., “W-band waveguide filters fabricated by laser micromachining and 3-D printing,” *IEEE Trans. Microw. Theory Techn.*, vol. 64, no. 8, pp. 2572–2580, Aug. 2016.
- [7] K. Iguchi, M. Tsuji, and H. Shigesawa, “Negative coupling between TE10 and TE20 modes for use in evanescent-mode bandpass filters and their field-theoretic CAD,” in *Proc. IEEE MTT-S Int. Microw. Symp. Dig.*, 1994, vol. 2, pp. 727–730.
- [8] S. Amari and U. Rosenberg, “Characteristics of cross (bypass) coupling through higher/lower order modes and their applications in elliptic filter design,” *IEEE Trans. Microw. Theory Techn.*, vol. 53, no. 10, pp. 3135–3141, Oct. 2005.
- [9] S. Amari, U. Rosenberg, and J. Bornemann, “Singlets, cascaded singlets and non-resonating node model for advanced modular design of elliptic filters,” *IEEE Microw. Wireless Compon. Lett.*, vol. 14, no. 5, pp. 237–239, May 2004.
- [10] G. Macchiarella, G. G. Gentili, C. Tomassoni, S. Bastioli, and R. V. Snyder, “Design of waveguide filters with cascaded singlets through a synthesis-based approach,” *IEEE Trans. Microw. Theory Techn.*, vol. 68, no. 6, pp. 2308–2319, Jun. 2020.
- [11] G. Macchiarella, G. G. Gentili, and L. Accatino, “Stopband singlet: A novel structure implementing resonating couplings,” *IEEE Microw. Compon. Lett.*, vol. 30, no. 5, pp. 473–476, May 2020.
- [12] Y. Xiao, P. Shan, K. Zhu, H. Sun, and F. Yang, “Analysis of a novel singlet and its application in THz bandpass filter design,” *IEEE Trans. THz Sci. Technol.*, vol. 8, no. 3, pp. 312–320, May 2018.
- [13] M. Esmaili and J. Bornemann, “Substrate integrated waveguide triplepassband dual-stopband filter using six cascaded singlets,” *IEEE Microw. Wireless Compon. Lett.*, vol. 24, no. 7, pp. 439–441, Jul. 2014.
- [14] U. Rosenberg, S. Amari, and J. Bornemann, “Inline TM110-mode filters with high design flexibility by utilizing bypass couplings of nonresonating TE10/01 modes,” *IEEE Trans. Microw. Theory Techn.*, vol. 51, no. 6, pp. 1735–1742, Jun. 2003.
- [15] M. A. Chaudhary and M. M. Ahmed, “Inline waveguide pseudo-elliptic filters using non-resonating modes with folded-waveguide resonators,” *IEEE Access*, vol. 9, pp. 140841–140852, 2021.
- [16] S. Bastioli, “Nonresonating mode waveguide filters,” *IEEE Microw. Mag.*, vol. 12, no. 6, pp. 77–86, Oct. 2011.
- [17] A. Vosough, A. A. Brazález, Y. Li, and Z. S. He, “A compact mass-producible E-band bandpass filter based on multi-layer waveguide technology,” in *Proc. 14th Eur. Conf. Antennas Propag.*, 2020, pp. 1–5.
- [18] X. Xu, M. Zhang, J. Hirokawa, and M. Ando, “E-band plate-laminated waveguide filters and their integration into a corporate-feed slot array antenna with diffusion bonding technology,” *IEEE Trans. Microw. Theory Techn.*, vol. 64, no. 11, pp. 3592–3603, Nov. 2016.
- [19] X. Zhang, C. Jin, and M. Gao, “Isosceles right triangular waveguides,” in *Proc. Int. Appl. Comput. Electromagn. Soc. Symp.*, 2017, pp. 1–2.
- [20] A. Morán-López, J. A. Ruiz-Cruz, J. Córcoles, J. R. Montejo-Garai, and J. M. Rebolgar, “Analytical expressions of the Q-factor for the complete resonant mode spectrum of the equilateral triangular waveguide cavity,” *Electron. Lett.*, vol. 55, pp. 944–947, Aug. 2019.
- [21] A. Morán-López, J. Córcoles, J. A. Ruiz-Cruz, J. R. Montejo-Garai, and J. M. Rebolgar, “Electromagnetic scattering at the waveguide step between equilateral triangular waveguides,” *Adv. Math. Phys.*, vol. 2016, Jul. 2016, Art. no. 2974675.
- [22] S. Bastioli and R. V. Snyder, “Quasi-elliptic evanescent-mode filters using non-resonating mode waveguide cavities,” *Int. J. Microw. Wireless Technol.*, vol. 7, pp. 211–218, Jun. 2015.
- [23] U. Rosenberg, S. Amari, J. Bornemann, and R. Vahldieck, “Compact pseudo-highpass filters formed by cavity and iris resonators,” in *Proc. 34th Eur. Microw. Conf.*, 2004, pp. 985–988.
- [24] J. Hong and M. J. Lancaster, *Microstrip filters for RF/Microwave Applications*. New York, NY, USA: Wiley, 2001.
- [25] X. Zhao, O. Glubokov, and J. Oberhammer, “A silicon-micromachined waveguide platform with axial ports for integrated sub-THz filters,” *IEEE Trans. Microw. Theory Techn.*, vol. 70, no. 2, pp. 1221–1232, Feb. 2022.